J. Fluid Mech. (1985), *vol.* 161, *pp.* 1–25
Printed in Great Britain

Instability of capillary jets with thermocapillarity

By J.-J. XU AND S. H. DAVIS
Department of Engineering Sciences and Applied Mathematics, Northwestern University, Evanston, IL 60201

(Received 2 April 1984 and in revised form 31 January 1985)

Long axisymmetric liquid zones are subject to axial temperature gradients which induce steady viscous flows driven by thermocapillarity. The approximately parallel flow in a cylindrical zone is examined for linearized instabilities. Capillary, surface-wave and thermal modes are found. Capillary breakup can be retarded or even suppressed for small Prandtl number and large Biot number B, which measures heat transfer from the liquid to the surrounding atmosphere. In the limiting case $B \to \infty$ the zone becomes an *isothermal* jet subject to axial 'wind stress' on its interface. It is then possible to suppress capillary breakup entirely so that one can maintain long coherent jets.

1. Introduction

It has been known since the time of Rayleigh (1879) that circular static inviscid liquid jets are unstable to axisymmetric disturbances having small axial wavenumber. The same instability is present in viscous jets (Chandrasekhar 1961). Observation has shown that this capillary instability, driven by surface-tension forces on the jet interface, leads to the breakup of the jet into droplets.

This knowledge has been essential for many applications ranging from the design of sprays to the design of inkjet printers. The behaviour of liquid bridges can be the controlling step in foam mechanics and multiphase displacement in the flow through porous media. In these cases the surface tension might not be constant but may depend on phase concentration or temperature. The containless processing of single crystals in the float-zone configuration involves the melting of a zone in a solid rod and its recrystallization. The liquid zone is a non-isothermal liquid bridge subject to axial temperature gradients.

A number of experimental observations (Chun & Wuest 1978, 1979; Schwabe *et al.* 1978) have documented the existence of steady flows generated by thermocapillarity. Here fluid flows from hot toward cold on the interface and returns along the axis due to the presence of endwalls on the zone. This flow can be *approximately* a parallel flow with a cylindrical interface (Xu & Davis 1983). The study of the instability of this flow is the object of the present work. Clearly, capillary instability (Rayleigh 1879; Chandrasekhar 1961) is possible. Surface-wave (Smith & Davis 1983*b*) and thermal (Smith & Davis 1983*a*) instabilities should be possible. New modes may appear. We wish to identify these and so determine the onset of oscillations that indicate a transition from steady flow to travelling-wave instabilities. The origin of these oscillations is currently the subject of considerable discussion. In an attempt to study possible instability mechanisms without the technical complications of involved basic states, Smith & Davis (1983*a*, *b*) have examined planar layers having surface-wave and thermal instabilities respectively. Xu & Davis (1984) have

examined thermal modes on axisymmetric zones in which surface deformation is absent.

In the present work we wish to examine liquid zones subject to axial temperature gradients which induce steady axial flows that are susceptible to time-periodic instabilities. Among the important results that emerge from this analysis is the fact that capillary instabilities can be greatly retarded or even suppressed by surface-wave instabilities (Smith & Davis 1983*b*) that couple surface deflection and the underlying shear. This is particularly effective for small Prandtl number and large Biot number B. B measures the heat transfer from the liquid into the surrounding gas. In the limit $B \to \infty$ we have an isothermal jet subject to a constant 'wind stress' τ (equal to the surface-tension gradient). For τ large enough the surface-wave instabilities (Miles 1960; Smith & Davis 1982) may eradicate completely the tendency for capillary breakup. Thus very long coherent zones can be produced. These zones are subject to the surface-wave instabilities that might lead to finite-amplitude permanent waves, but are not expected to lead to breakup.

2. Formulation

Consider an infinitely long axisymmetric liquid bridge bounded laterally by a free surface of mean radius a. The bridge is composed of an incompressible Newtonian liquid having viscosity μ, density ρ, specific heat c_p, thermal conductivity k and unit thermal surface conductance h. We write $\nu = \mu/\rho$ and $\kappa = k/\rho c_p$. The surface tension on the interface is σ.

The bridge, shown in figure 1, is described using a cylindrical coordinate system (r, θ, z) with the z-axis coinciding with the axis of the bridge; the corresponding velocity components are (u, v, w).

A constant temperature gradient $\mathrm{d}T/\mathrm{d}z = -b$, $b > 0$, is imposed along the axis of the bridge. The surface tension varies linearly with temperature:

$$\sigma = \sigma_0 - \gamma(T - T_0), \tag{2.1}$$

where T_0 is the temperature of the interface at $z = 0$, say. Here

$$\gamma = -\left.\frac{\mathrm{d}\sigma}{\mathrm{d}T}\right|_{T=T_0} > 0 \tag{2.2}$$

gives the rate of change of surface tension with temperature T.

We scale the governing equations consistent with isothermal capillary instabilities of a liquid using the following units: length $\sim a$, speed $\sim w_{**} = (\sigma_0/\rho a)^{\frac{1}{2}}$, pressure $\sim \sigma_0/a$, temperature difference $T - T_0 \sim ba$, surface tension $\sim \sigma_0$ and time $\sim (\rho a^3/\sigma_0)^{\frac{1}{2}}$. In addition to the velocity scale w_{**}, appropriate capillary breakup, there is another associated with thermocapillarity, viz $w_* = \gamma b a/\mu$ (see e.g. Sen & Davis 1982).

This choice of scaling, consistent with capillary instabilities, supposes that the zone is long enough to be susceptible to such breakups and that thermocapillary effects are 'superposed' on these. Xu & Davis (1984), in considering convective modes without interfacial deformation, try to isolate effects in shorter zones where breakup is forbidden and only the 'weaker' thermocapillary effects are present. Thus they use different scales for speed, pressure and time. In particular, their choice of pressure

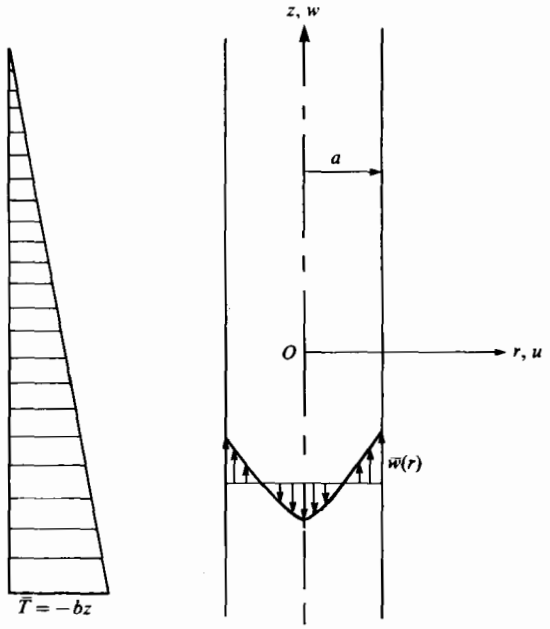

FIGURE 1. Sketch of the basic-state jet with the thermocapillary-induced axial-velocity profile.

scale γb reflects their view that the large mean capillary effects, scaled on pressure σ_0/a, should not be effective when breakup is forbidden.

As a result of the scaling, the following non-dimensional groups emerge:

$$S = \left(\frac{\rho a w_{**}}{\mu}\right)^2 \doteq \frac{\rho a \sigma_0}{\mu^2}, \tag{2.3a}$$

$$R_{\mathrm{B}} = \frac{\rho a w_*}{\mu} = \frac{\rho \gamma b a^2}{\mu^2}, \tag{2.3b}$$

$$P = \frac{\nu}{\kappa}, \quad B = \frac{ha}{k}. \tag{2.3c,d}$$

The parameter $S^{\frac{1}{2}}$ is the Reynolds number of capillary instabilities, and measures the influence of mean surface tension. The Reynolds number R_{B} measures the steady thermocapillary flow driven by the imposed axial temperature gradient. P is the Prandtl number and B is the surface Biot number that measures heat transfer from the liquid to the adjoining gas.

In terms of non-dimensional quantities, the governing equations are Navier–Stokes, continuity and energy:

$$u_t + uu_r + \frac{1}{r}vu_\theta + wu_z - \frac{1}{r}v^2 = -p_r + S^{-\frac{1}{2}}\left(\nabla^2 u - \frac{1}{r^2}u - \frac{2}{r}v_\theta\right), \tag{2.4a}$$

$$v_t + uv_r + \frac{1}{r}vv_\theta + wv_z + \frac{1}{r}uv = -\frac{1}{r}p_\theta + S^{-\frac{1}{2}}\left(\nabla^2 v - \frac{1}{r^2}v + \frac{2}{r}u_\theta\right), \tag{2.4b}$$

$$w_t + uw_r + \frac{1}{r}vw_\theta + ww_z = -p_z + S^{-\frac{1}{2}}\nabla^2 w, \tag{2.4c}$$

$$u_r+\frac{1}{r}u+\frac{1}{r}v_\theta+w_z=0, \tag{2.4d}$$

$$P\left(T_t+uT_r+\frac{1}{r}vT_\theta+wT_z\right)=S^{-\frac{1}{2}}\nabla^2T, \tag{2.4e}$$

where subscripts denote partial differentiation.

On the interface at $r=R(\theta,z,t)$ we have the kinematic, shear-stress, normal-stress and thermal boundary conditions:

$$u=R_t+\frac{1}{r}vR_\theta+wR_z, \tag{2.5a}$$

$$2\left(1+\frac{1}{r^2}R_\theta^2+R_z^2\right)^{-\frac{1}{2}}\left\{\frac{1}{r}R_\theta u_r-\frac{1}{r}R_\theta R_z(w_r+u_z)-\frac{1}{r^2}R_\theta(1+R_z^2)(u+v_\theta)+\frac{1}{r}R_\theta R_z^2w_z\right.$$
$$\left.+\frac{1}{2}\left(1+R_z^2+\frac{1}{r^2}R_\theta^2\right)\left[\frac{1}{r}u_\theta+v_r-\frac{1}{r}v-R_z\left(v_z+\frac{1}{r}w_\theta\right)\right]\right\}$$
$$=-S^{-\frac{1}{2}}R_{\mathrm{B}}\left\{\frac{1}{r}R_\theta T_r+\frac{1}{r}(1+R_z^2)T_\theta-\frac{1}{r}R_\theta R_zT_z\right\}, \tag{2.5b}$$

$$2\left(1+\frac{1}{r^2}R_\theta^2+R_z^2\right)^{-\frac{1}{2}}\left\{R_zu_r-\frac{1}{2r}R_\theta R_z\left(\frac{1}{r}u_\theta+v_r-\frac{1}{r}v\right)\right.$$
$$\left.+\tfrac{1}{2}(1-R_z^2)(w_r+u_z)-\frac{1}{2r}R_\theta\left(v_z+\frac{1}{r}w_\theta\right)-R_zw_z\right\}=-S^{-\frac{1}{2}}R_{\mathrm{B}}\{R_zT_r+T_z\}, \tag{2.5c}$$

$$-p+2S^{-\frac{1}{2}}\left(1+\frac{1}{r^2}R_\theta^2+R_z^2\right)^{-1}\left\{u_r-\frac{1}{r}R_\theta\left(\frac{1}{r}u_\theta+v_r-\frac{1}{r}v\right)\right.$$
$$\left.-R_z(w_r+u_z)+\frac{1}{r^3}R_\theta^2(u+v_\theta)+\frac{1}{r}R_\theta R_z\left(v_z+\frac{1}{r}w_\theta\right)+R_z^2w_z\right\}=K[1-S^{-1}R_{\mathrm{B}}T], \tag{2.5d}$$

where the curvature K satisfies

$$K=[R^2(1+R_z^2)+R_\theta^2]^{-\frac{3}{2}}\{RR_{zz}(R^2+R_\theta^2)+2R_\theta R_z(R_\theta R_z-RR_{\theta z})$$
$$-(1+R_z^2)(R^2+2R_\theta^2-RR_{\theta\theta})\}, \tag{2.5e}$$

$$\left(1+\frac{1}{r^2}R_\theta^2+R_z^2\right)^{-\frac{1}{2}}\left\{T_r-\frac{1}{r^2}R_\theta T_\theta-R_zT_z\right\}+B(T-T_{\mathrm{a}})=0. \tag{2.5f}$$

Equation (2.5a) is the kinematic condition, (2.5b,c) give the thermocapillary balances: shear stresses balance the surface-tension gradients. Equations (2.5d,e) give the balance between the normal stress and the curvature times the surface tension. Equation (2.5f) balances the heat flux across the interface, where $T_{\mathrm{a}}=T_{\mathrm{a}}(z)$ denotes the air temperature at the interface.

Finally, all physical quantities are bounded at $r=0$:

$$|u|,\ |v|,\ |w|,\ |p|,\ |T|<\infty \quad (r=0). \tag{2.6}$$

3. Basic state

The imposed axial temperature gradient drives a steady shear flow in the bridge as described by Xu & Davis (1983). For small capillary number Ca,

$$Ca=S^{-1}R_{\mathrm{B}}\ll 1, \tag{3.1}$$

i.e. for $S \gg 1$, this flow is nearly parallel and the zone has a nearly cylindrical interface. This approximate solution has the form

$$\bar{u}, \bar{v} \sim 0, \quad \bar{w} \sim \tfrac{1}{2}S^{-\frac{1}{2}}R_{\mathrm{B}}(r^2-\tfrac{1}{2}), \tag{3.2a, b}$$

$$\bar{p} \sim 1+2S^{-1}R_{\mathrm{B}}\,z, \quad \bar{T} \sim -z-\tfrac{1}{32}PR_{\mathrm{B}}(1-r^2)^2, \tag{3.2c, d}$$

$$R \sim 1, \quad T_a(z) = -z. \tag{3.2e, f}$$

4. Disturbance equations

All dependent variables ϕ are written as the sum of a steady basic state $\bar{\phi}$ and a disturbance ϕ'. These are substituted into the governing system (2.5) and linearized in primed quantities. Then the basic-state quantities, which appear in the coefficients, are replaced by their approximate versions (3.2).

One term that appears in the linearized normal-stress boundary condition (2.5*d*) is

$$[1-S^{-1}R_{\mathrm{B}}\,\bar{T}(1,z)]\,(R'+R'_{zz}+R'_{\theta\theta}) \approx [1+S^{-1}R_{\mathrm{B}}\,z]\,(R'+R'_{zz}+R'_{\theta\theta}).$$

As argued by Smith & Davis (1983*a*), this term can be treated as one with constant coefficients as long as disturbances vary rapidly in z compared to Ca^{-1}. This is a restriction on the axial wavenumber α soon to be introduced, viz

$$2\pi R_B/\alpha S \ll 1. \tag{4.1}$$

In this case the term (4.1) is replaced by $R'+R'_{zz}+R'_{\phi\phi}$, and we neglect $S^{-1}R_B z$ compared with unity.

Having made the 'slowly varying' assumption just discussed, the linearized disturbance equations have coefficients depending only on r and can be analysed using normal modes:

$$\phi'(r,\theta,z,t) = \hat{\phi}(r)\,\mathrm{e}^{\mathrm{i}(\alpha z+m\theta-\sigma t)}, \tag{4.2a}$$

where α and (integer) m are respectively the axial and azimuthal wavenumbers, and the eigenvalue

$$\sigma = \omega+\mathrm{i}\nu \tag{4.2b}$$

contains the growth rate ν and the angular frequency ω. In terms of these normal modes, the linearized disturbance system takes the form

$$\left\{\mathrm{D}\mathrm{D}_*-\alpha^2-\frac{m^2}{r^2}-\mathrm{i}\alpha R_{\mathrm{B}}\,W_0(r)+\mathrm{i}S^{\frac{1}{2}}\sigma\right\}\hat{u}-\frac{2\mathrm{i}m}{r^2}\hat{v} = S^{\frac{1}{2}}\mathrm{D}\hat{p}, \tag{4.3a}$$

$$\left\{\mathrm{D}\mathrm{D}_*-\alpha^2-\frac{m^2}{r^2}-\mathrm{i}\alpha R_{\mathrm{B}}\,W_0(r)+\mathrm{i}S^{\frac{1}{2}}\sigma\right\}\hat{v}+\frac{2\mathrm{i}m}{r^2}\hat{u} = \frac{\mathrm{i}mS^{\frac{1}{2}}}{r}\hat{p}, \tag{4.3b}$$

$$\left\{\mathrm{D}_*\,\mathrm{D}-\alpha^2-\frac{m^2}{r^2}-\mathrm{i}\alpha R_{\mathrm{B}}\,W_0(r)+\mathrm{i}S^{\frac{1}{2}}\sigma\right\}\hat{w}-R_{\mathrm{B}}\,W_0'(r)\,\hat{u} = \mathrm{i}\alpha S^{\frac{1}{2}}\hat{p}, \tag{4.3c}$$

$$\left\{\mathrm{D}_*\,\mathrm{D}-\alpha^2-\frac{m^2}{r^2}-\mathrm{i}\alpha PR_{\mathrm{B}}\,W_0(r)+\mathrm{i}PS^{\frac{1}{2}}\sigma\right\}\hat{T} = P^2S^{\frac{1}{2}}R_{\mathrm{B}}\,T_0'(r)\,\hat{u}-PS^{\frac{1}{2}}\hat{w}, \tag{4.3d}$$

$$\mathrm{D}_*\,u+\frac{\mathrm{i}m}{r}\hat{v}+\mathrm{i}\alpha\hat{w} = 0, \tag{4.3e}$$

$$\hat{u}(1)+[\mathrm{i}\sigma-\mathrm{i}\alpha S^{-\frac{1}{2}}R_{\mathrm{B}}\,W_0(1)]\,\hat{R} = 0, \tag{4.3f}$$

$$\mathrm{D}\hat{v}(1)-\hat{v}(1)+\mathrm{i}m\hat{u}(1)+\mathrm{i}mS^{-\frac{1}{2}}R_{\mathrm{B}}\hat{T}(1)=0, \tag{4.3g}$$

$$\mathrm{D}\hat{w}(1)+\mathrm{i}\alpha\hat{u}(1)+S^{-\frac{1}{2}}R_{\mathrm{B}}[\mathrm{i}\alpha\hat{T}(1)+\hat{R}]=0, \tag{4.3h}$$

$$-\hat{p}(1)+2S^{-\frac{1}{2}}\mathrm{D}\hat{u}(1)-(1-\alpha^2-m^2)\hat{R}-S^{-1}R_{\mathrm{B}}[2\mathrm{i}\alpha\hat{R}+\hat{T}(1)]=0, \tag{4.3i}$$

$$\mathrm{D}\hat{T}(1)+B\hat{T}(1)-[\tfrac{1}{4}PR_{\mathrm{B}}-\mathrm{i}\alpha]\hat{R}=0, \tag{4.3j}$$

$$|\hat{u}|,\ |\hat{v}|,\ |\hat{w}|,\ |\hat{p}|,\ |\hat{T}|<\infty \quad (r=0). \tag{4.3k}$$

Here
$$W_0(r)=\tfrac{1}{2}(r^2-\tfrac{1}{2}),\quad T_0(r)=-\tfrac{1}{32}(1-r^2)^2 \tag{4.4a, b}$$

and
$$\mathrm{D}\equiv\frac{\mathrm{d}}{\mathrm{d}r},\quad \mathrm{D}_*\equiv\frac{\mathrm{d}}{\mathrm{d}r}+\frac{1}{r}; \tag{4.5}$$

primes also denote $\mathrm{d}/\mathrm{d}r$.

We shall solve the system (4.3) for general values of the parameters. Given that $r=0$ is a singular point of the cylindrical coordinate system, we must exclude this point from the integration interval. We do this in two alternative ways. (i) We take the correct conditions valid for $r=0$ and apply them at $r=\delta_1\ll 1$ to obtain a two-point eigenvalue problem. (ii) We expand all dependent variables about $r=0$ and obtain asymptotic representations that ensure regularity and give a linearly independent set of solutions. By applying these conditions at $r=\delta_2\ll 1$ we obtain a two-point eigenvalue problem. We find that the methods give equivalent results. For $\delta_1=0.001$ or $\delta_2=0.01$ we obtain five-place accuracy.

Finally, given the formulation of the two-point boundary-value problem we use the code SUPORT written by Scott & Watts (1975, 1977) to integrate the system (4.3). In the system (4.3) the approximate basic state (3.2) occurs as coefficients; it is an adequate approximation only if $Ca\ll 1$. We must thus ensure that this inequality holds in all physically significant situations.

5. Special cases

5.1. $R_{\mathrm{B}}=O(1)$ as $S\to\infty$: the inviscid capillary jet

In this limit the viscosity of the fluid approaches zero, which makes thermocapillarity effective only in a thin free-surface boundary layer of thickness $O(S^{-\frac{1}{2}})$; the characteristic equation is regular, however. Thus we regain the inviscid characteristic equation associated with Rayleigh breakup (Rayleigh 1879):

$$\left.\begin{aligned}&\omega=0,\\ &\nu=\pm\left[\frac{I_1(\alpha)}{I_0(\alpha)}\alpha(1-\alpha^2)\right]^{\frac{1}{2}}\end{aligned}\right\}\quad (0\leqslant\alpha\leqslant 1), \tag{5.1a}$$

$$\left.\begin{aligned}&\omega=\pm\left[\frac{I_1(\alpha)}{I_0(\alpha)}\alpha(\alpha^2-1)\right]^{\frac{1}{2}},\\ &\nu=0\end{aligned}\right\}\quad (1\leqslant\alpha<\infty), \tag{5.1b}$$

where I_k is the modified Bessel function of the first kind. The result (5.1) corresponds to the axisymmetric mode $m=0$; all non-axisymmetric modes $m\neq 0$ correspond to stable disturbances, as shown by their characteristic equations

$$\left.\begin{aligned}&\omega=\pm\left[\frac{I_m'(\alpha)}{I_m(\alpha)}\alpha(\alpha^2+m^2-1)\right]^{\frac{1}{2}},\\ &\nu=0.\end{aligned}\right\} \tag{5.2}$$

Note that the inviscid formulae (5.1) and (5.2) emerge as regular limits of the viscous characteristic equations. However, there may be eigenvalues of the viscous problem that have no inviscid limit.

It is useful in what follows to plot ω and ν for mode $m = 0$ as shown in figure 2. The figure ν versus α is symmetric about the α-axis for $S \to \infty$. Instability occurs only for $m = 0$ and for α in the range $(0, \alpha_c)$, where α_c is the cutoff wavenumber:

$$\alpha_c = 1 \quad (S \to \infty). \tag{5.3a}$$

The maximum growth rate ν_M occurs for $\alpha = \alpha_M$, the maximizing wavenumber:

$$\alpha_M \approx 0.69, \quad \nu_M \approx 0.34 \quad (S \to \infty). \tag{5.3b}$$

Note that $\alpha = 0$ and $\alpha = 1$ are branch points of the characteristic equation for mode $m = 0$.

We shall call the branch $m = 0$, $0 \leqslant \alpha \leqslant \alpha_c$, $\nu > 0$ the characteristic equation of the *capillary mode* $W_0^{(c)}$. We shall say that the *surface-wave mode* $W_0^{(-)}$ corresponds to the branch $m = 0$, $\alpha_c < \alpha < \infty$, $\omega < 0$, while the remainder of the mode $m = 0$ is called the *hydrodynamic mode* $W_0^{(+)}$. In the limit $S \to \infty$, $W_0^{(+)}$ and $W_0^{(-)}$ are neutral in the range $\alpha_c < \alpha < \infty$. This classification will be explained later.

5.2. $R_B = 0$, $S < \infty$: *the viscous capillary jet*

In this limit we regain the result for the viscous isothermal capillary jet (Chandrasekhar 1961):

$$2\alpha^2(\alpha^2+\delta^2)\frac{I_1'(\alpha)}{I_0(\alpha)}\left[1-\frac{2\alpha\delta}{\alpha^2+\delta^2}\frac{I_1(\alpha)}{I_1(\delta)}\frac{I_1'(\delta)}{I_1'(\alpha)}\right]-(\alpha^4-\delta^4) = S\frac{\alpha I_1(\alpha)}{I_0(\alpha)}(1-\alpha^2), \tag{5.4a}$$

where

$$\delta^2 = \alpha^2 - i\sigma S^{\frac{1}{2}}. \tag{5.4b}$$

Equations (5.4) correspond to the mode $m = 0$, and all $m \neq 0$ modes correspond to stable disturbances.

Figure 2 shows ω and ν for various values of S. The point $\alpha = \alpha_B$ corresponds to the maximum value of wavenumber at which $\omega = 0$ (see figure 2*a*) and equivalently the α at which the mode $m = 0$ has its (negative) growth rate ν split (see figure 2*a*). The points $\alpha = 0$ and $\alpha = \alpha_B$ are branch points of the dispersion relation, and again

$$\alpha_c = 1 \quad (S < \infty).$$

Note that α_M increases as S increases, so that smaller viscosity corresponds to shorter maximizing waves. Also note that α_B decreases with increasing values of S. Given that the viscosity is non-zero, the surface-wave mode $W_0^{(-)}$ and the hydrodynamic mode $W_0^{(+)}$ both decay (and have equal decay rates) for $\alpha \geqslant \alpha_B$.

5.3. $B \to \infty$, P, $R_B = O(1)$: *the 'flying jet'*

This is the general dynamical *isothermal* problem in which the basic flow field is established by external forces (e.g. 'wind' blowing over the cylinder with a prescribed shear stress τ equal to the imposed thermocapillary gradient γb).

In the limit $B \to \infty$, (4.3*j*) yields that $\hat{T}(1) = 0$, so that thermal perturbations vanish on the interface and the thermal field does not influence the hydrodynamic instability. Here R_B is the measure of the 'wind stress' (Smith & Davis 1982).†

† As noted by Smith & Davis (1982), the 'slowly varying' approximation discussed in §4 is not required for such isothermal cases.

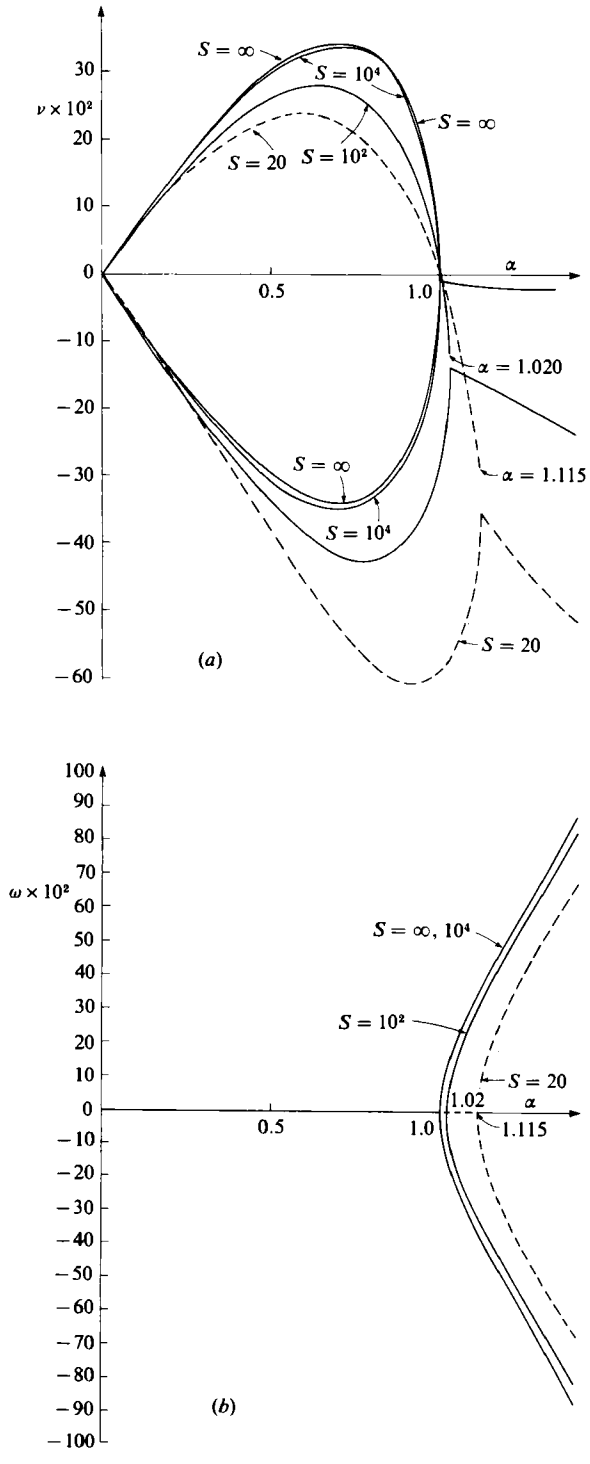

FIGURE 2. (*a*) Growth rate ν versus axial wavenumber α for the isothermal jet for the mode $m = 0$ for $R_B = 0$ and various S. (*b*) Frequency ω versus axial wavenumber α for the isothermal jet for the mode $m = 0$ for $R_B = 0$ and various S.

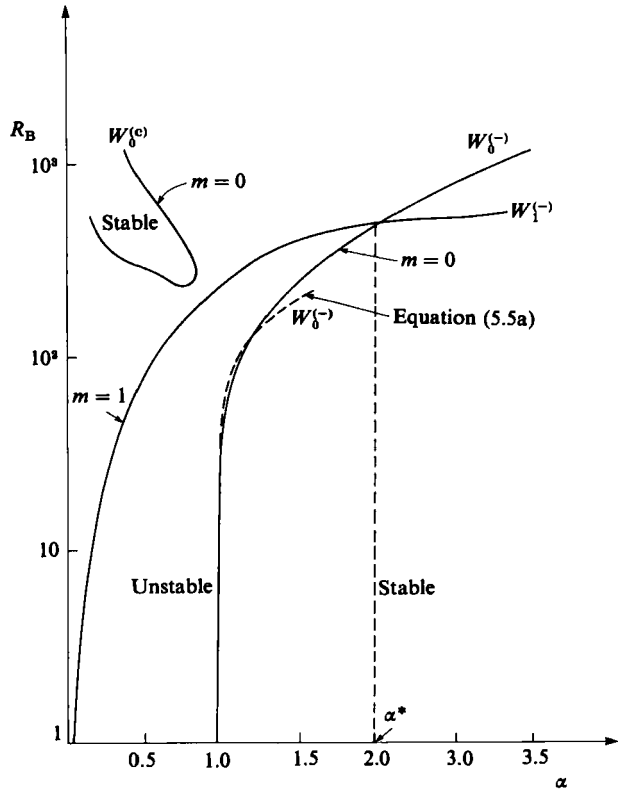

FIGURE 3. Neutral curves for the isothermal jet with $S = 10^4$ including the modes $W_0^{(c)}$, $W_0^{(-)}$ and $W_1^{(-)}$.

For small R_B, regular perturbation theory gives the cutoff conditions for mode $m = 0$:

$$\alpha_c \sim 1 + 0.1300 R_B^2 S^{-1} + O(R_B^4), \tag{5.5a}$$

$$\omega_c \sim -0.3759 R_B S^{-\frac{1}{2}} + O(R_B^3), \tag{5.5b}$$

where $\omega_c \equiv \omega(\alpha_c)$. Figure 3 shows the results for α_c as a function of R_B for $S = 10^4$ from numerical computations compared with the result (5.5*a*), the latter being accurate for $R_B < 100$ (i.e. $R_B S^{-1} < 1$).

Figure 4 shows ω and ν for $S = 10^4$. Note that, since $R_B \neq 0$, the decay rates for $W_0^{(+)}$ and $W_0^{(-)}$ differ in the range $\alpha_c < \alpha < \infty$. Further, there is a smooth transition from $W_0^{(c)}$ to $W_0^{(-)}$ as α increases.

As R_B increases from zero to 100, the cutoff wavenumber α_c increases monotonically. However, when R_B is somewhat larger than 200 the curve of ν versus α dips below the axis for $\alpha < \alpha_c$, as shown in figure 4(*a*), thus producing a sequence of *three crossings*: say α_1, α_2 and α_c, the largest of these. The capillary mode $W_0^{(c)}$ is confined to a small range of α, $0 < \alpha < \alpha_1$, and α_M decreases as R_B increases. Thus the presence of the basic-state shear flow inhibits the Rayleigh capillary breakup; *longer coherent zones are thus possible if there is flow in the zone.*

The presence of the background shear is also responsible for the appearance of a new instability, attributable to coupled shear/interface effects (Miles 1960; Smith & Davis 1982). This is seen in figure 4(*a*); when the three crossings are present a second local maximum of ν appears in (α_2, α_c) at $\alpha = \alpha_M' > 1$. For example, from figure 4(*a*)

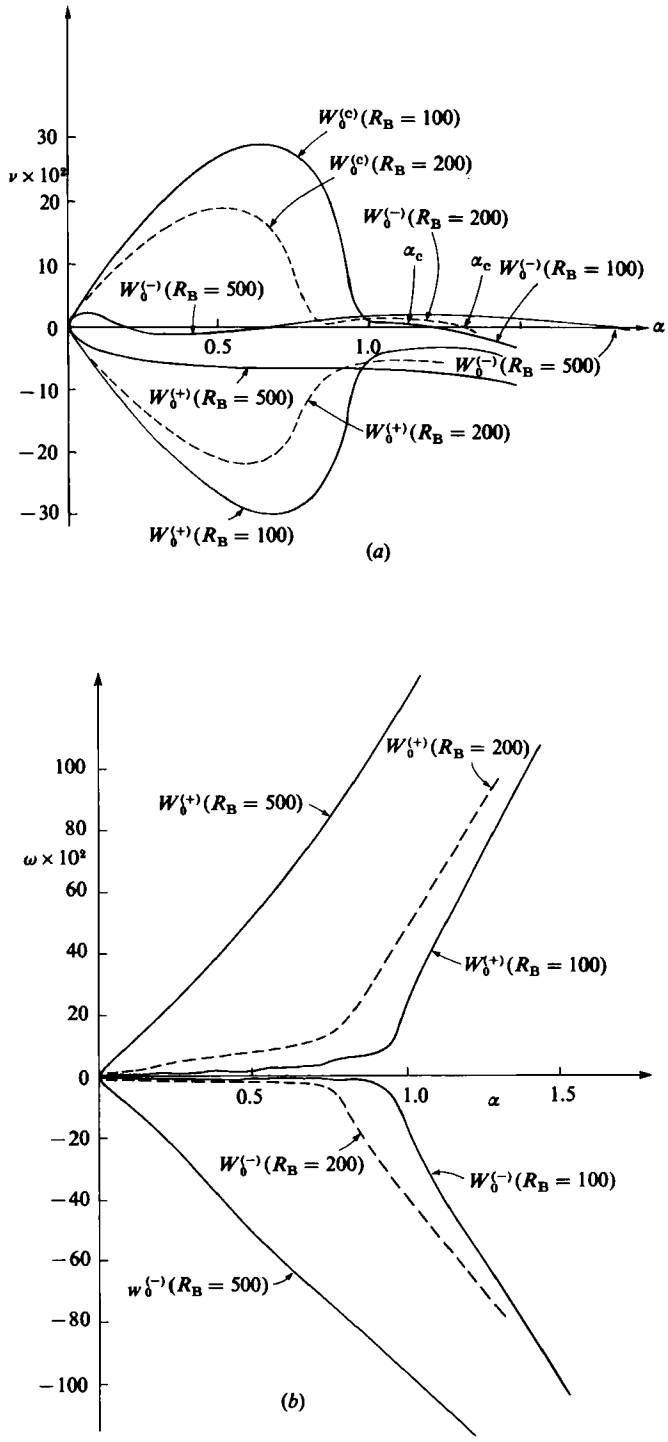

FIGURE 4. (*a*) Growth rate ν versus axial wavenumber α for the isothermal jet for the mode $m = 0$ for $S = 10^4$ and various R_B. (*b*) Frequency ω versus axial wavenumber α for the mode $m = 0$ for $S = 10^4$ and various R_B.

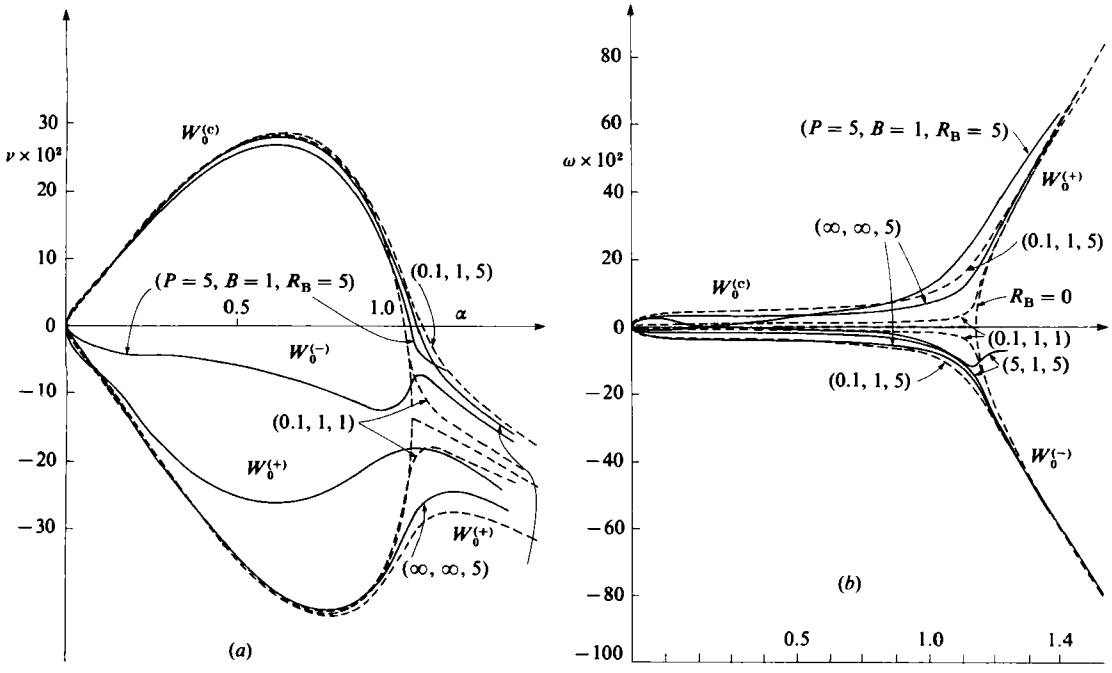

FIGURE 5. (*a*) Growth rate ν versus axial wavenumber α for the non-isothermal jet mode $m = 0$ for $S = 10^2$ and various R_B, P and B. (*b*) Frequency ω versus axial wavenumber α for the non-isothermal jet for mode $m = 0$ for $S = 10^2$ and various R_B, P and B.

for $R_B = 200$ we get $\alpha_M = 0.53$, $\alpha'_M = 1.0$, $\nu_M = 0.19$ and $\nu'_M = 0.84 \times 10^{-2}$. The zone would be unstable to shear waves emerging from mode $W_0^{(-)}$, these waves propagating in the direction *opposite* to the imposed surface flow. This is consistent with the small-α analysis of Smith & Davis (1982) on planar isothermal sheared layers having return-flow profiles. Notice also that the frequencies of these surface-wave modes are substantially larger than those of the capillary mode as shown in figure 4(*b*). The presence of this hydrodynamic instability makes the longer zone possible, though the resulting configuration is unsteady. Notice in figure 4(*a*) for, say, $R_B = 500$ that $W_0^{(c)}$ has a second neutral point, so that there exists another neutral branch in the range $0 < \alpha < 1$. This is shown in figure 3 for mode $m = 0$.

We now turn to mode $m = 1$. Since $R_B \neq 0$ the non-axisymmetric mode $m = 1$ is sometimes unstable, the neutral curve being shown in figure 3 emerging from the origin. We see in figure 3 for $0 < \alpha < 1$ that the $m = 0$ mode $W_0^{(c)}$ dominates, for $1 < \alpha < \alpha^* \approx 2.0$ the $m = 0$ surface-wave mode $W_0^{(-)}$ dominates, while for $\alpha > \alpha^*$ the $m = 1$ surface-wave mode $W_1^{(-)}$ is most dangerous.

6. Thermocapillary instabilities

In analysing non-isothermal systems we must recall *two* restrictions on the physical validity of our theory. First, we have assumed a nearly cylindrical zone, which is guaranteed by (3.1), a restriction that applies even for the isothermal 'flying' jet of §5.3. Secondly, we must enforce the 'slowly varying' restriction (4.1), which limits the wavenumber for the validity of the theory, viz

$$\alpha \gg 2\pi R_B S^{-1}. \tag{6.1}$$

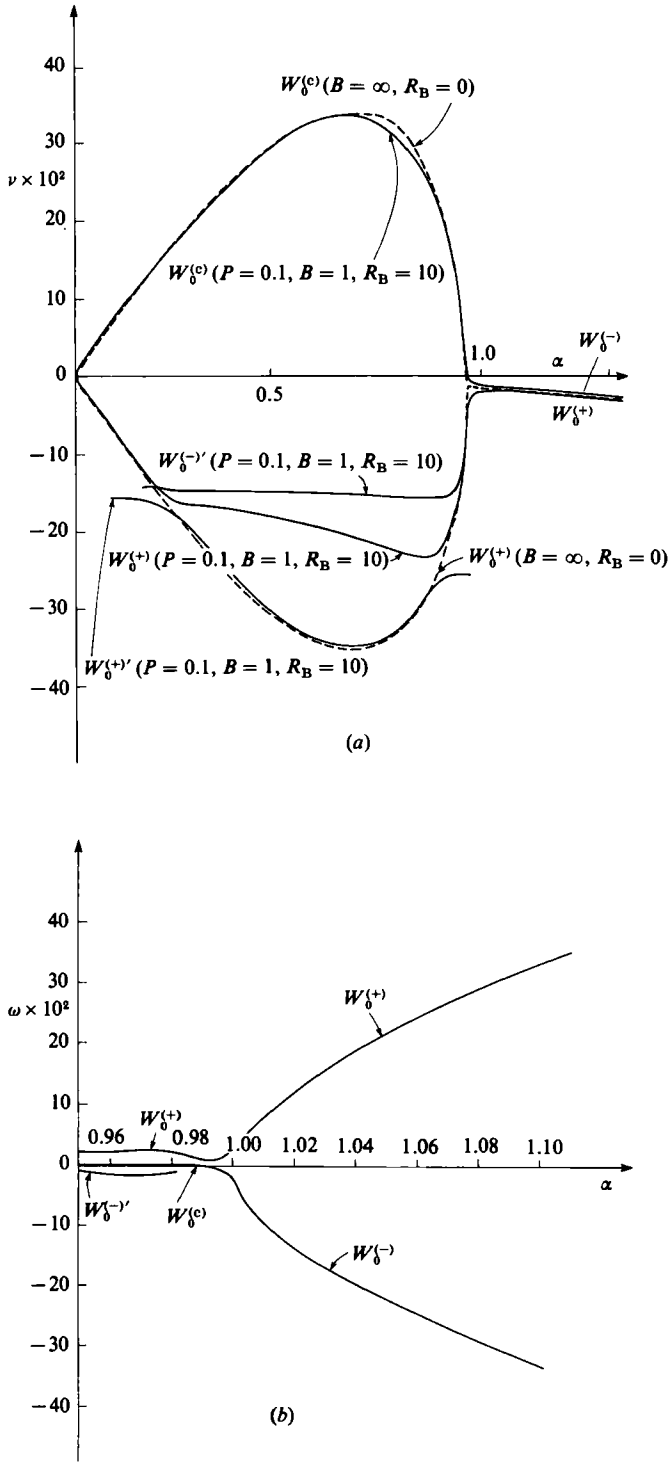

FIGURE 6. (*a*) Growth rate ν versus axial wavenumber α for the non-isothermal jet for the mode $m = 0$ for $S = 10^4$, $P = 0.1$, $B = 1$ and $R_B = 10$. (*b*) Frequency ω versus axial wavenumber α for mode $m = 0$ for $S = 10^4$, $P = 0.1$, $B = 1$ and $R_B = 10$.

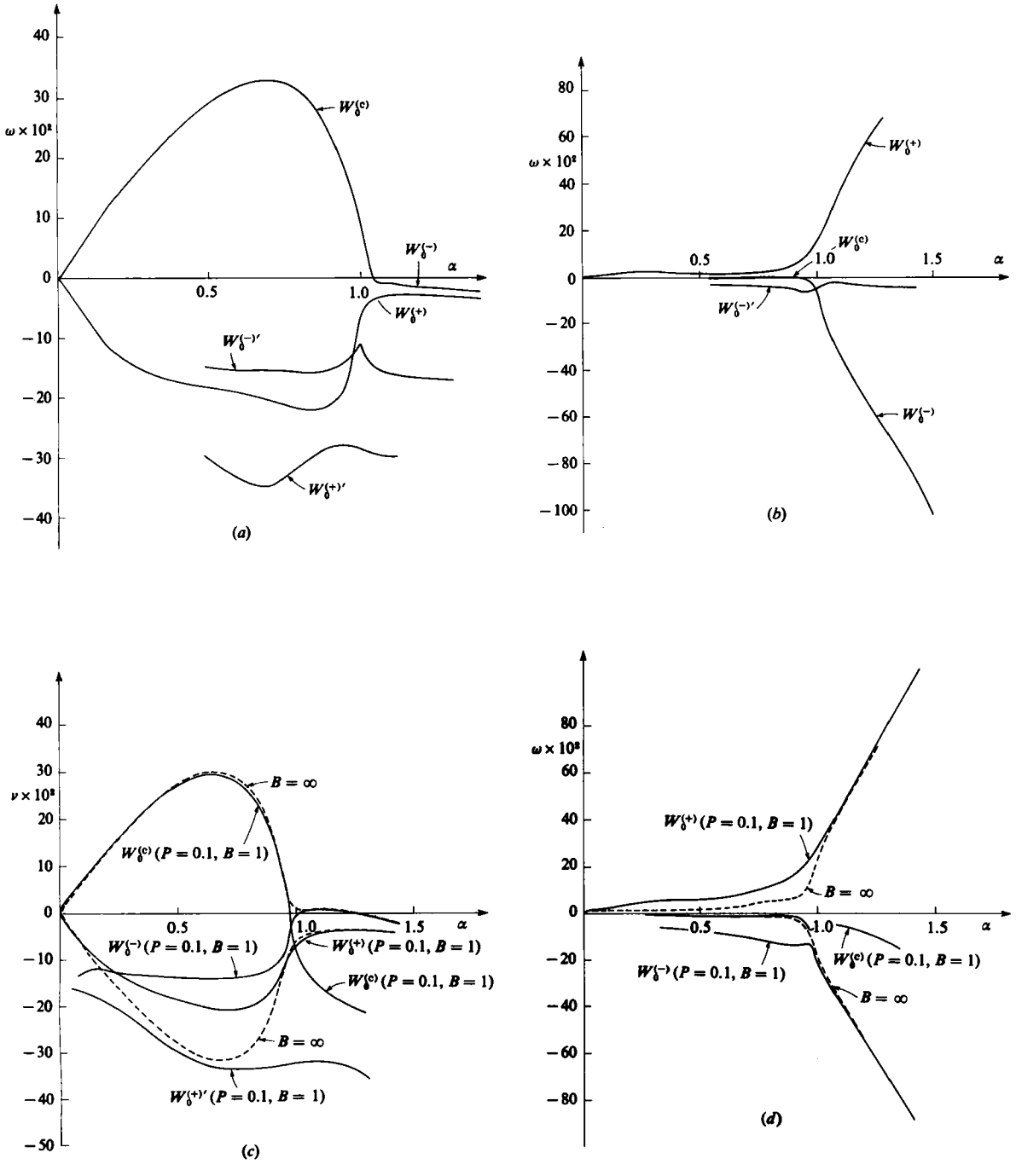

FIGURE 7 (*a*)–(*d*). For caption see next page.

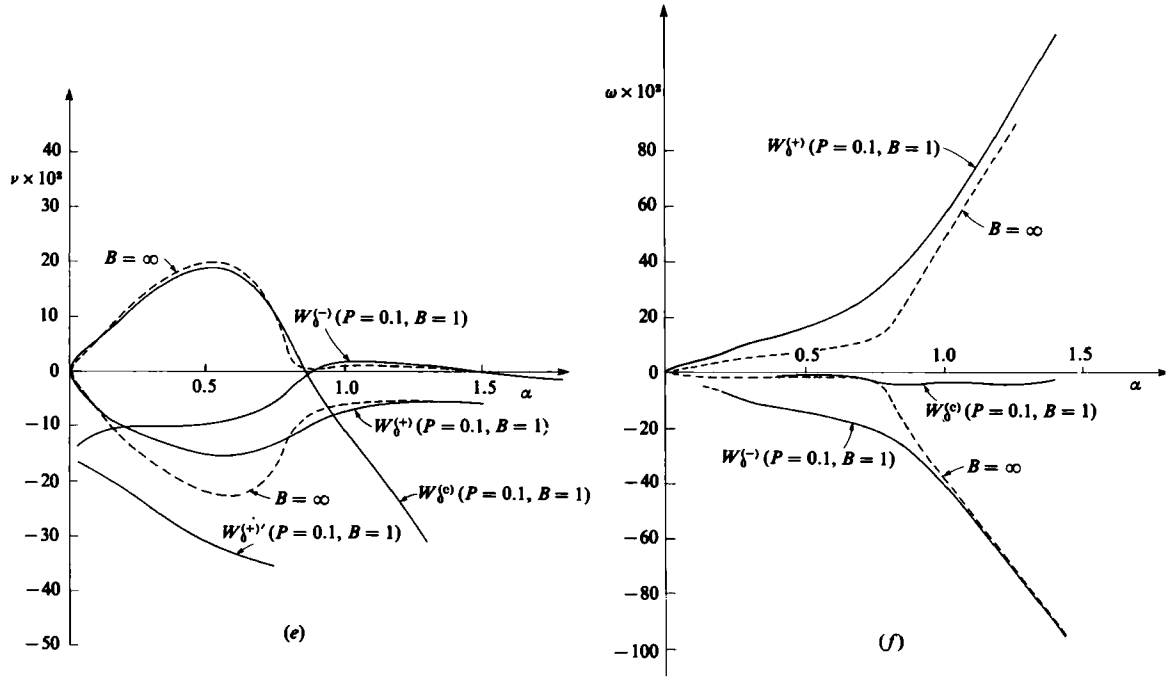

FIGURE 7. (*a*) Growth rate ν versus axial wavenumber α for the non-isothermal jet for the mode $m = 0$ for $S = 10^4$, $P = 0.1$, $B = 1$ and $R_B = 40$. (*b*) Frequency ω versus axial wavenumber α for the non-isothermal jet for the mode $m = 0$ for $S = 10^4$, $P = 0.1$, $B = 1$ and $R_B = 40$. (*c*) Growth rate ν versus axial wavenumber α for the non-isothermal jet for the mode $m = 0$ for $S = 10^4$, $P = 0.1$, $B = 1$ and $R_B = 100$. (*d*) Frequency ω versus axial wavenumber α for the non-isothermal jet for the mode $m = 0$ for $S = 10^4$, $P = 0.1$, $B = 1$ and $R_B = 100$. (*e*) Growth rate ν versus axial wavenumber α for the non-isothermal jet for the mode $m = 0$ for $S = 10^4$, $P = 0.1$, $B = 1$ and $R_B = 200$. (*f*) Frequency ω versus axial wavenumber α for the non-isothermal jet for the mode $m = 0$ for $S = 10^4$, $P = 0.1$, $B = 1$ and $R_B = 200$.

In the discussion to follow we ignore the restriction (6.1) in order to examine fully the complicated structure of the neutral curves as parameters vary and to test our numerics against asymptotic formulae for small α. However, we only infer *physical* content when the inequality (6.1) is enforced.

We now turn to cases $B < \infty$ and $R_B \neq 0$. For B, P, $R_B = O(1)$ there are long-wave instabilities $\alpha \to 0$. We find by regular perturbation theory that

$$\omega + \mathrm{i}\nu \sim \pm(\tfrac{1}{2}R_B S^{-1}\alpha)^{\frac{1}{2}}(1-\mathrm{i}) + \tfrac{1}{4}PS^{-\frac{1}{2}}R_B B^{-1}\alpha + O(\alpha^{\frac{3}{2}}), \tag{6.2}$$

so that the frequency ω, which is zero for $S \to \infty$ or $R_B \to 0$, splits near $\alpha = 0$ into a pair of curves with a vertical tangents as shown in figure 5(*b*). Likewise, near $\alpha = 0$ the growth rate splits into two curves with vertical tangents near $\alpha = 0$ as shown in figure 5(*a*), which corresponds to the case $S = 100$ and $B = 1$. For $R_B = 5$, (3.1) gives $Ca = 0.05$. The numerical computation agrees with the form (6.1) to within 5×10^{-4} for the case $P = 0.1$, $S = 100$, $R_B = 10$, $B = 1$, $\alpha = 0.01$. Figure 6 shows the frequency ω and growth rate ν corresponding to the case $S = 10^4$, $P = 0.1$, $B = 1$ and $R_B = 10$. Both figures 5 and 6 show that, if the values of P and R_B are not too large, then the modes $W_0^{(c)}$ and $W_0^{(-)}$ are smoothly connected, consistent with the dynamic isothermal case. However, as either P or R_B becomes larger, the situation changes. First of all, the modes $W_0^{(c)}$ and $W_0^{(-)}$ split as shown in figure 5 for the case $P = 5$,

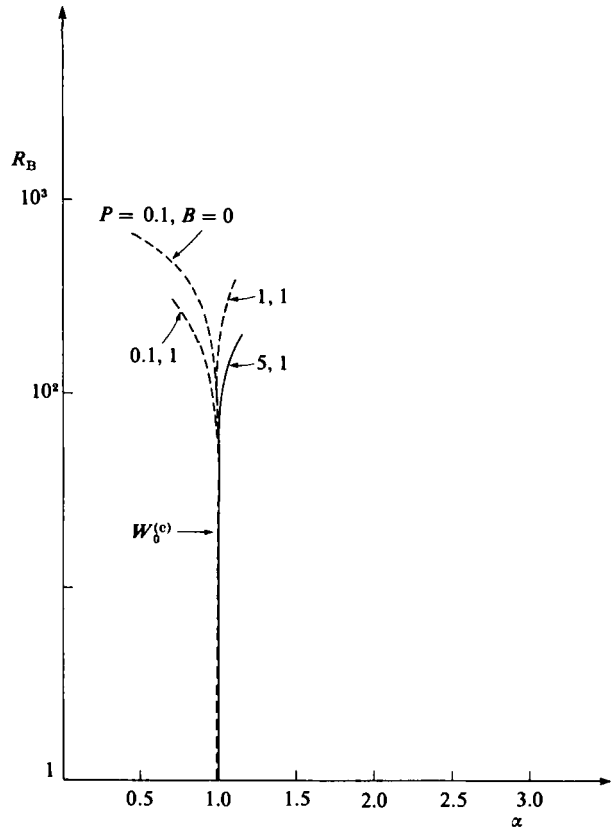

FIGURE 8. Neutral curves near $\alpha = 1$ for the non-isothermal jet for the mode $W_0^{(c)}$ for $S = 10^4$ and various P and B.

$B = 1, S = 10^2$ and $R_B = 5$. This splitting process is also seen in figures 6 and 7, which correspond to the cases $P = 0.1, B = 1, S = 10^4, R_B = 10$, and 40, 100, 200 respectively. Figure 6 shows that as R_B is increased from 0 to 10 the characteristic curve of mode $W_0^{(+)}$ will give birth to an additional branch $W_0^{(+)\prime}$ while the characteristic curve of mode $W_0^{(-)}$ will also have a sub-branch $W_0^{(-)\prime}$. As R_B increases further, the branch $W_0^{(+)\prime}$ separates further from $W_0^{(+)}$ (as shown in figures 6*a*, 7*a*, *c*, *e*); however, the branch $W_0^{(-)\prime}$ and the curves of $W_0^{(c)}$ and $W_0^{(-)}$ will evolve as shown in figures 6(*b*) and 7(*b*, *d*, *f*). Thus the curves of modes $W_0^{(c)}$ and $W_0^{(-)}$ remain separated. Figure 8 shows the neutral curve near $\alpha = 1$ of $W_0^{(c)}$ for various values of B and P. Figures 9 and 10 show the neutral curve near $\alpha = 1$ of $W_0^{(-)}$ for various values of B and P. Furthermore, for a fixed R_B as P increases, the mode $W_0^{(+)}$ may become unstable as shown in figures 11 and 12, which correspond to the cases $S = 10^4$, $B = 1$, $R_B = 100$, $P = 1$ and $P = 5$ respectively. Note that the instability of $W_0^{(+)}$ is a *new instability* caused by increasing Marangoni number $M_B \equiv PR_B$ and does not exist in the isothermal hydrodynamic case. Hence it is a *hydrothermal* instability, which differs from the instabilities identified by Smith & Davis (1983*a*, *b*). Figure 13(*a*) shows the neutral curves of this instability as a function of P; figure 13(*b*) shows the Reynolds number R_B of the neutral wave with $\alpha = 1$ versus P and B. Finally, figure 14 shows for the mode $W_0^{(c)}$ that the maximum growth rate ν_M and maximizing wavenumber α_M decrease with increasing R_B; these also increase with S. Thus the presence of the shear

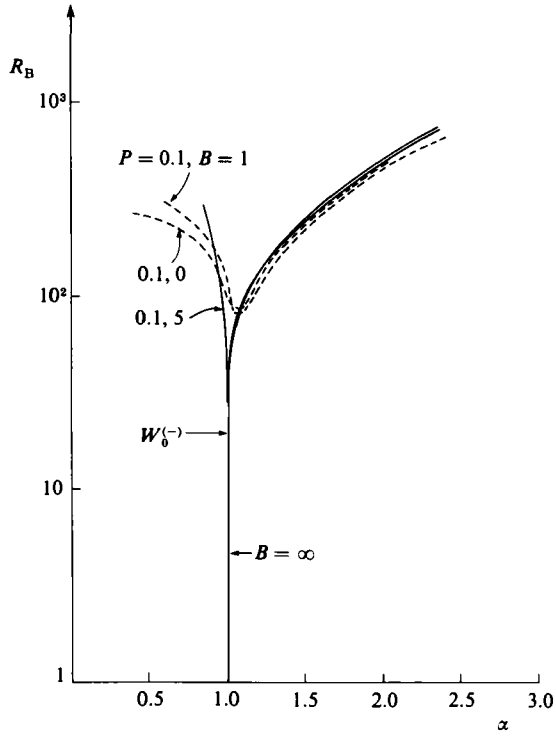

FIGURE 9. Neutral curves near $\alpha = 1$ for the non-isothermal jet for the mode $W_0^{(-)}$ for $S = 10^4$, $P = 0.1$ and various B.

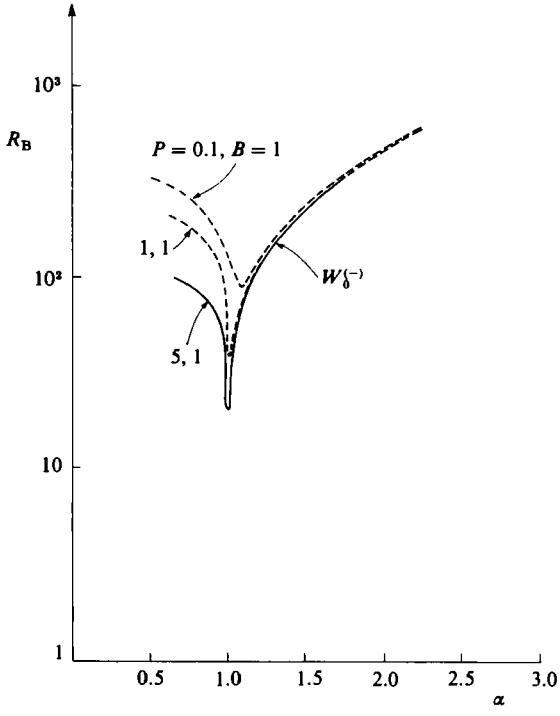

FIGURE 10. Neutral curves near $\alpha = 1$ for the non-isothermal jet for the mode $W_0^{(-)}$ for $S = 10^4$, $B = 1$ and various P.

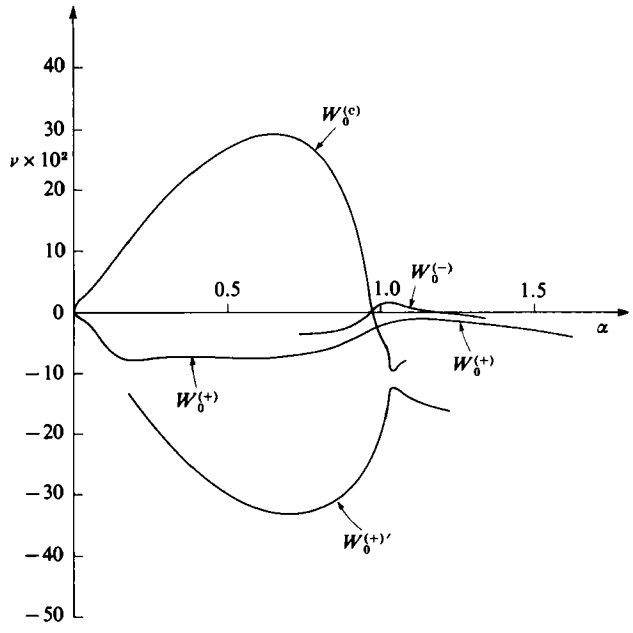

FIGURE 11. Growth rate ν versus axial wavenumber α for the non-isothermal jet for the mode $m = 0$ for $S = 10^4$, $P = 1$, $B = 1$ and $R_B = 100$.

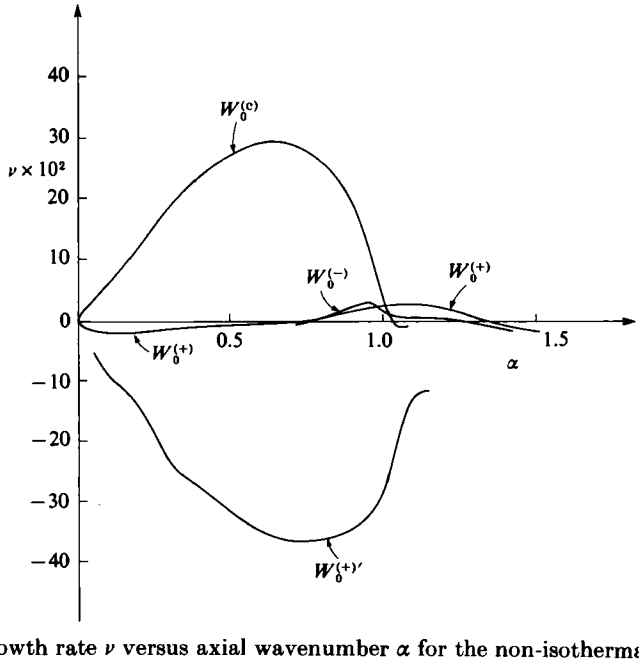

FIGURE 12. Growth rate ν versus axial wavenumber α for the non-isothermal jet for the mode $m = 0$ for $S = 10^4$, $P = 5$, $B = 1$ and $R_B = 100$.

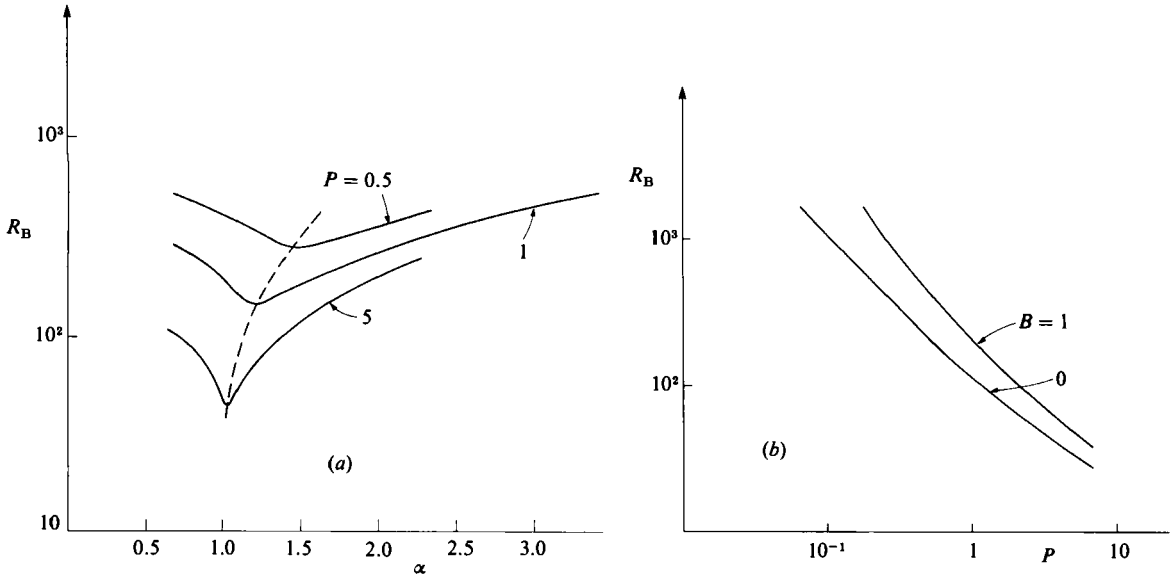

FIGURE 13. (*a*) Neutral curves near $\alpha = 1$ for the non-isothermal jet for the mode $W_0^{(+)}$ for $S = 10^4$ and $B = 1$ for various P. (*b*) Neutral points at $\alpha = 1$ versus P for the non-isothermal jet for the mode $W_0^{(+)}$ for $S = 10^4$ and $B = 0$ or $B = 1$.

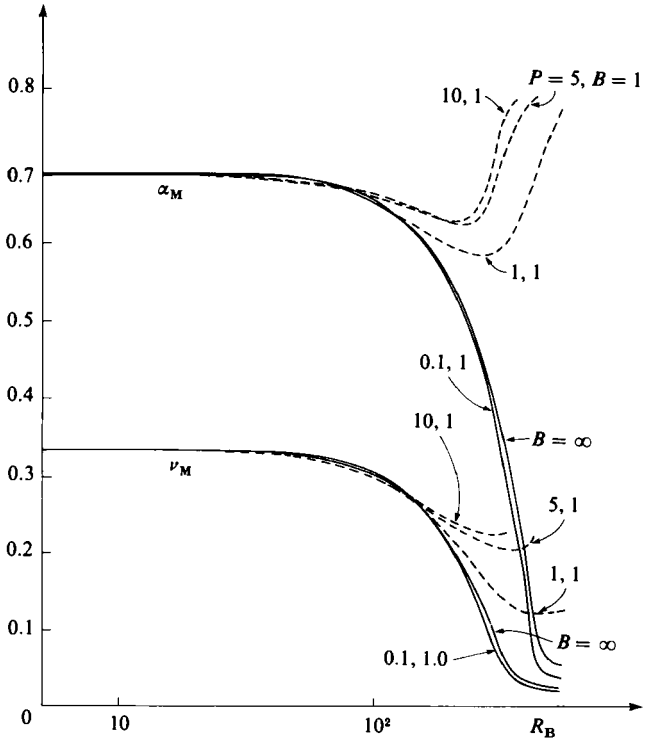

FIGURE 14. Maximum growth rate ν_M and maximizing wavenumber α_M versus R_B for the non-isothermal jet for the mode $W_0^{(c)}$ for $S = 10^4$ for various P and B.

gives rise to new instabilities that suppress the capillary instability, allowing larger zones to persist. Relatively speaking, ν_M and α_M are not very sensitive to variations in the thermal parameters P and B if $R_B \leqslant 100$. For example, α_M and ν_M change by 0.58 and 1.39% as B varies from unity to ∞ for $S = 10^4$, $P = 0.1$ and $R_B = 100$. Similarly α_M and ν_M change by 2.27 and 2.32% as P varies from 10^{-1} to 10 for $S = 10^4$, $B = 1$ and $R_B = 100$.

For the non-axisymmetric mode $m = 1$ the eigenvalues are quite close to those of the general isothermal case. However, there is a non-uniform limit for $\alpha \to 0$, and the growth rates for $\alpha \to 0$ differ between the isothermal and non-isothermal cases. $W_1^{(-)}$ grows while $W_1^{(+)}$ decays for the isothermal case and $\alpha \to 0$. $W_1^{(-)}$ decays while $W_1^{(+)}$ grows for the non-isothermal case and $\alpha \to 0$. Figures 15–21 show the neutral curves for different cases and ranges of α. The neutral curve of mode $W_1^{(+)}$ seems to be confined to very low wavenumbers or very high Reynolds numbers R_B. We could not find it elsewhere.

Therefore, in summary, there exist several important instability mechanisms or unstable modes in the thermocapillary problem:

(I) capillary mode $W_0^{(c)}$;
(II) surface-wave modes $W_0^{(-)}$ and $W_1^{(-)}$;
(III) thermal mode $W_0^{(+)}$.

Figures 17–21 show that, when P is small, modes II are important, whereas when P is large mode III emerges in the range $1 < \alpha < 3$. In all cases, mode I, as long as it exists, dominates small α.

At this stage, given the structure we have found for the instability modes, we must enforce the inequality (6.1); there is physical content only in this range.

7. Discussion and conclusions

We consider an infinitely long capillary jet of radius unity subject to an axial temperature gradient of unit magnitude. Thermocapillarity causes an approximately parallel axial flow driven on the interface by surface-tension gradients and returning along the axis.

The instabilities of this dynamic state are governed by four parameters: R_B, S, P and B. The Reynolds number of the thermocapillary flow is R_B, while $S^{-\frac{1}{2}}$ is the Reynolds number of the (isothermal) capillary jet; it measures the mean surface tension. P is the Prandtl number of the liquid. B is the Biot number that measures heat transfer from the liquid jet into the atmosphere.

In the limit $B \to \infty$ all thermal perturbations on the liquid–gas interface vanish. Thus all instabilities are isothermal in nature (and are independent of P). The model presumes that the interface is nearly cylindrical, so that surface tension must be large enough according to the inequality (3.1). The physical system is thus equivalent to an isothermal viscous jet subject to wind stress τ equal to the thermocapillary gradient γb of the basic state. This 'flying jet' is susceptible to both capillary instabilities (Rayleigh 1879) as well as those generated by interactions of the underlying shear with interface deformations (Miles 1960; Smith & Davis 1982). For $R_B = 0$, there is only the capillary mode $W_0^{(c)}$, which grows only for the case $m = 0$ in the range $0 < \alpha < \alpha_c = 1$. As R_B increases, the growing $W_0^{(c)}$ modes travel slowly in the direction opposite to the surface flow. The cutoff axial wavenumber α_c increases with R_B. The capillary mode is accompanied by a surface-wave mode $W_0^{(-)}$, whose branch is connected to that of $W_0^{(c)}$ but is distinguished by the group velocity C_g. There

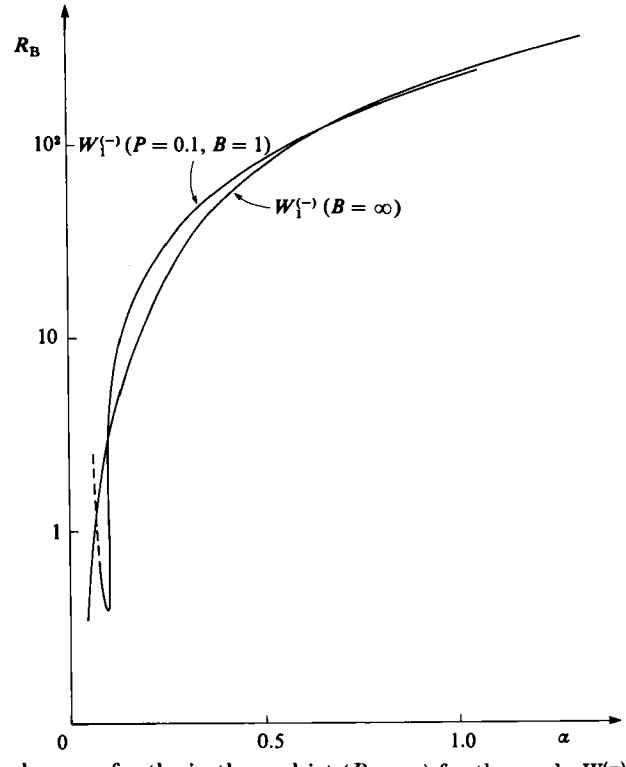

FIGURE 15. Neutral curves for the isothermal jet ($B = \infty$) for the mode $W_1^{(-)}$ with $S = 10^4$ and the non-isothermal jet for the mode $W_1^{(-)}$ with $B = 1$, $P = 0.1$ and $S = 10^4$.

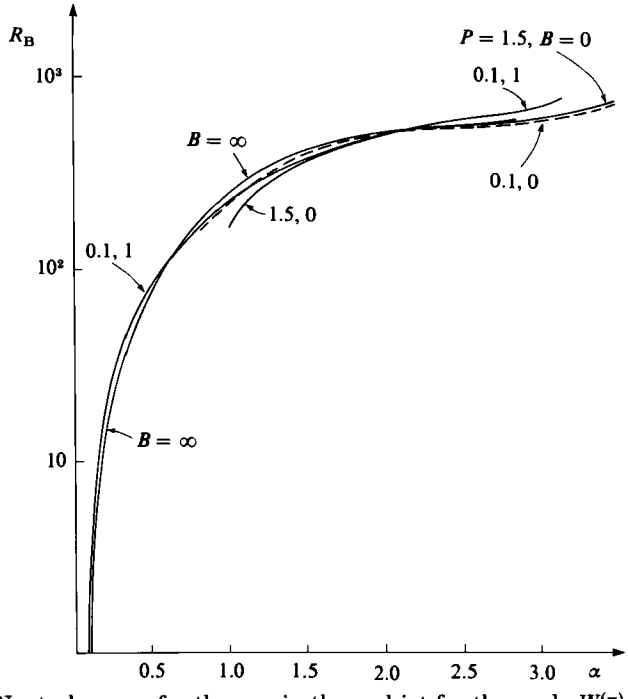

FIGURE 16. Neutral curves for the non-isothermal jet for the mode $W_1^{(-)}$ for $S = 10^4$ with (i) $B \to \infty$, (ii) $B = 1$, $P = 0.1$, (iii) $B = 0$, $P = 0.1$ and (iv) $B = 0$, $P = 1.5$.

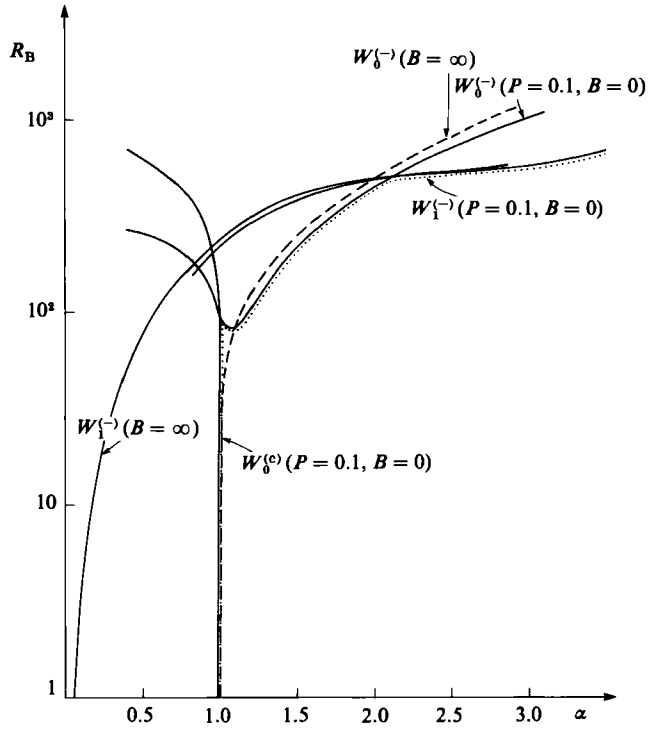

FIGURE 17. Neutral curves for the non-isothermal jet for $S = 10^4$, $B = 0$ and $P = 0.1$ and for the isothermal jet ($B = \infty$) for $S = 10^4$.

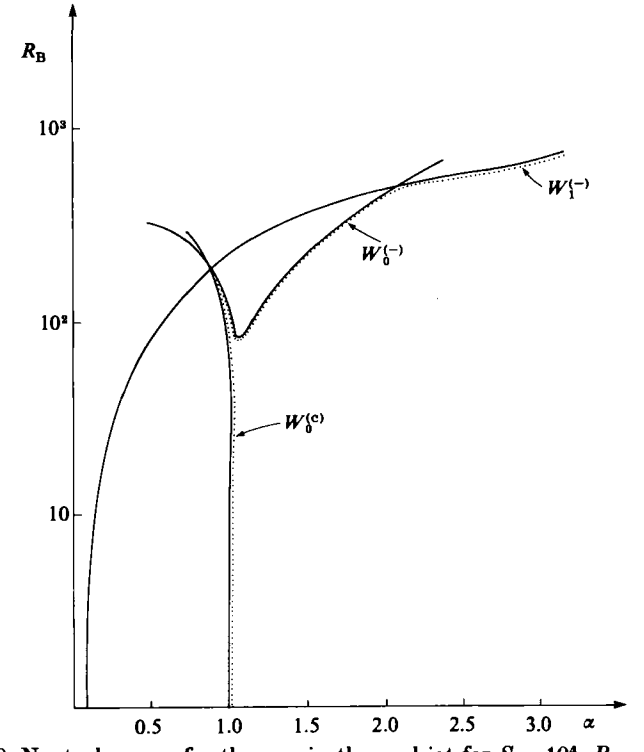

FIGURE 18. Neutral curves for the non-isothermal jet for $S = 10^4$, $B = 1$ and $P = 0.1$.

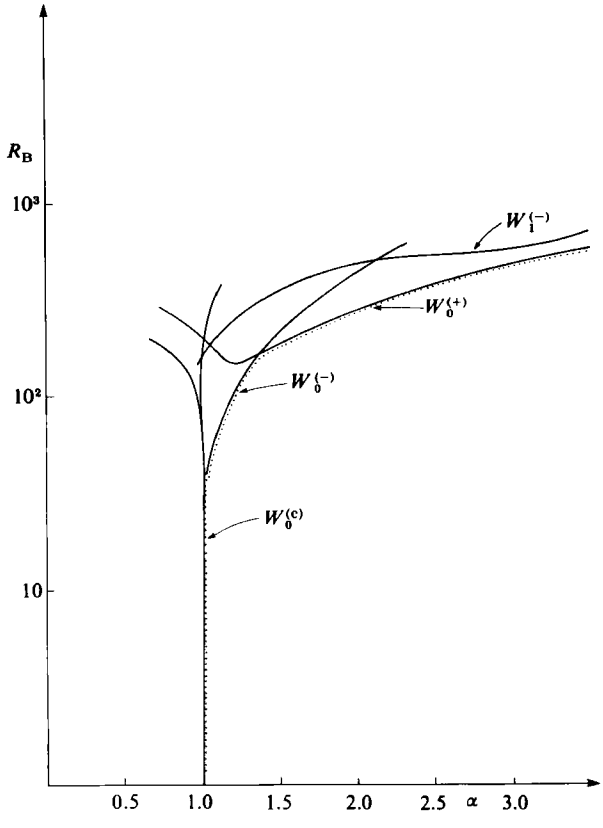

FIGURE 19. Neutral curves for the non-isothermal jet for $S = 10^4$, $B = 1$ and $P = 1$.

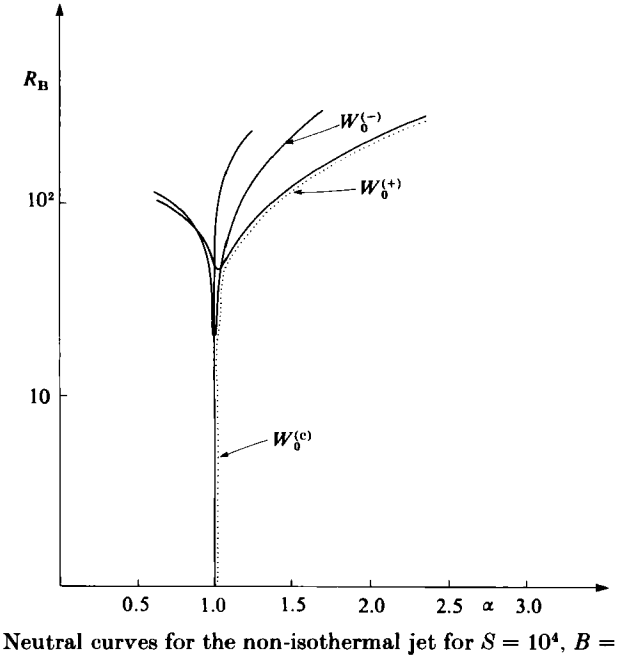

FIGURE 20. Neutral curves for the non-isothermal jet for $S = 10^4$, $B = 1$ and $P = 5$.

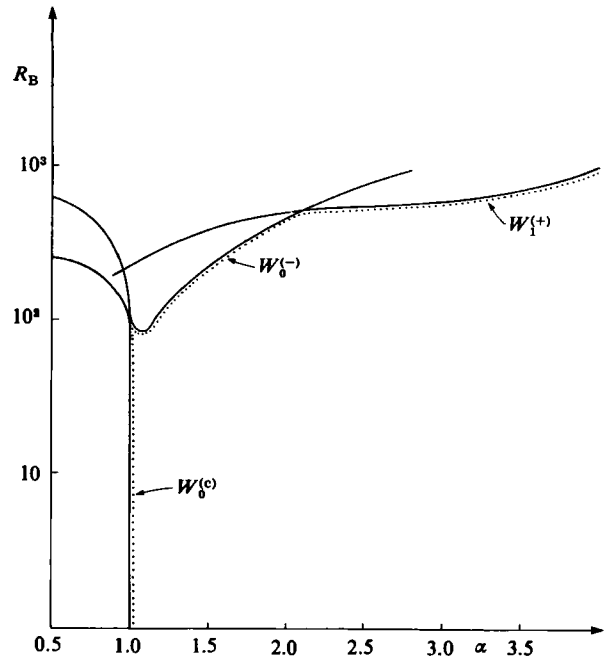

FIGURE 21. Neutral curves for the non-isothermal jet for $S = 10^4$, $B = 0$ and $P = 0.1$.

is a maximum of $dC_g/d\alpha$ at $\alpha = \alpha_B$; we call $W_0^{(c)}$ that for $\alpha < \alpha_B$ and $W_0^{(-)}$ that for $\alpha > \alpha_B$.

As R_B is increased, α_c increases, but the maximizing wavenumber α_M and its corresponding maximum growth rate ν_M *decrease*. Finally, for $S = 10^4$ and, say, $R_B = 500$, the ν versus α curve exhibits *three* zeros as shown in figure 4. For $0 < \alpha < \alpha_1$, say, there is a capillary instability. For $\alpha_1 < \alpha < \alpha_2$, say, no modes grow. For $\alpha_2 < \alpha < \alpha_c$ there is a surface-wave instability. Thus the basic-state flow suppresses the capillary instability into a small range $0 < \alpha < \alpha_1$, with α_1 decreasing with R_B, but allows a new surface-wave mode (Miles 1960; Smith & Davis 1982). Owing to the basic-state flow, a very long liquid jet can persist (without breaking up into droplets) though it has fast instability waves on it propagating in the direction opposite to the surface flow. Even when $R_B = 200$, the neutral curve exhibits two local maxima indicating the presence of the two instabilities. All these modes are axisymmetric ($m = 0$). When α is large enough, the $m = 1$ mode $W_1^{(-)}$ for surface-wave instabilities becomes predominant. Figure 3 shows that this occurs for $\alpha > 2.0$ (approximately) for $S = 10^4$.

When $B < \infty$ thermal perturbations are present on the interface, the Prandtl number P appears in the stability criteria and new thermal instabilities become possible. In addition to the restriction (3.1), we now require that the variables vary slowly along the zone. Thus the restriction (4.1) limits the axial wavenumber to be 'not too small'. When B is not too small and P is not too large the modes $m = 0$ resemble those of the 'flying jet'. $W_0^{(c)}$ is smoothly connected to $W_0^{(-)}$ to $\alpha = \alpha_B$. Again $W_0^{(c)}$ propagates slowly while $W_0^{(-)}$ propagates rapidly. As either R_B or P increases, the modes $W_0^{(c)}$ and $W_0^{(-)}$ split; the neutral curve for $W_0^{(c)}$ passes through the point $\alpha = 1$, $R_B = 0$ and depends strongly on P and B as shown in figure 8. The neutral curve of $W_0^{(-)}$ does not pass through the point $\alpha = 1$, $R_B = 0$, and for short waves (e.g. $\alpha > 1.25$ for $S = 10^4$, $B = 1$, $P = 0.1$) is not strongly dependent on P and B as shown in figures 9 and 10.

As in the case of the isothermal ($B \to \infty$) 'flying jet', capillary instabilities can be suppressed by the action of the basic-state flow and its instabilities. Figure 14 shows that this suppression is most significant for B large and/or P small. For example, if $P = 0.1$, $B = 1$ and $S = 10^4$ the capillary instability is completely suppressed if $R_B > 400$, though the restriction (4.1) prevents the analysis from being valid for $\alpha \to 0$. All we can say is that some degree of suppression exists.

As P increases and B decreases, a new instability arises. The mode $W_0^{(+)}$, a function of P and B, becomes less stable as B is decreased from infinity, and finally becomes unstable for P large enough, B small enough and R_B large enough. This represents a thermal instability resulting in waves that travel in the direction opposite to the surface flow.

There are also two spiral modes $m = 1$ for $W_1^{(-)}$ and $W_1^{(+)}$ which are rapidly travelling waves in the directions opposite to and along the surface flow respectively. These have group velocities similar to their isothermal counterparts. However, for $\alpha \ll 1$, $W_1^{(+)}$ is unstable while $W_1^{(-)}$ is stable. For larger α (say $\alpha > 2$) $W_1^{(-)}$ is close to that of the isothermal 'flying jet'.

In summary then, we have the following behaviours.

(i) The capillary mode $W_0^{(c)}$ is a wave that travels slowly along the axis opposite to or along the surface flow, and is directly related to the capillary instability of static cylinders studied by Rayleigh (1879) and Chandrasekhar (1961). This mode can be suppressed for B large and/or P small by instabilities of the basic-state flow driven by thermocapillarity. As a special case, the limit $B \to \infty$ retrieves the 'flying jet' having the same property.

(ii) The surface-wave mode $W_0^{(-)}$ is a wave that travels rapidly along the axis opposite to the surface flow. It is controlled by R_B and is only weakly dependent on parameters P and B if $\alpha > 1.2$, and so is the axisymmetric analogue of the instability identified by Miles (1960) and Smith & Davis (1982) and studied in the planar thermocapillary layer by Smith & Davis (1983*a*).

(iii) The thermal mode $W_0^{(+)}$ is a wave that travels rapidly along the axis along the surface flow. It is controlled by the basic-state Marangoni number $M_B \equiv PR_B$ and is distinct from the instabilities identifed by Smith & Davis (1983*a*, *b*). The critical value of M_B approaches infinity as $B \to \infty$ or $P \to 0$, and becomes dominant for P large and B small.

(iv) The surface-wave mode $W_1^{(-)}$ is a spiral wave that travels along the axis opposite to the surface flow and in either azimuthal direction. It is controlled by R_B and is weakly dependent on P and B.

In conclusion, for small P, the neutral curve is made up of segments from $W_0^{(c)}$, $W_0^{(-)}$ and $W_1^{(-)}$. For large P the neutral curve is made up of segments from $W_0^{(c)}$ and $W_0^{(+)}$. Thus liquid bridges of finite length may be long or short, but will usually be subject to oscillatory instabilities of surface-wave or thermal type.

This work was supported by the National Aeronautics and Space Administration, Materials-Processing-in-Space Program, Contract NAS8-33881.

REFERENCES

CHANDRASEKHAR, S. 1961 *Hydrodynamic and Hydromagnetic Stability*. Oxford University Press.

CHUN, C.-H. & WUEST, W. 1978 *Acta Astronautica* **5**, 681.

CHUN, C.-H. & WUEST, W. 1979 *Acta Astronautica* **6**, 1073.

MILES, J. W. 1960 *J. Fluid Mech.* **8**, 593.
RAYLEIGH, LORD 1879 *Proc. Lond. Math. Soc.* **10**, 4.
SCHWABE, D., SCHARMANN, A., PREISSER, F. & OEDER, R. 1978 *J. Crystal Growth* **43**, 305.
SCOTT, M. R. & WATTS, H. A. 1975 *Sandia Labs Rep.* SAND 75-0198, Albuquerque.
SCOTT, M. R. & WATTS, H. A. 1977 *SIAM J. Numer. Anal.* **14**, 40.
SEN, A. K. & DAVIS, S. H. 1982 *J. Fluid Mech.* **121**, 163.
SMITH, M. K. & DAVIS, S. H. 1982 *J. Fluid Mech.* **121**, 187.
SMITH, M. K. & DAVIS, S. H. 1983*a* *J. Fluid Mech.* **132**, 119.
SMITH, M. K. & DAVIS, S. H. 1983*b* *J. Fluid Mech.* **132**, 145.
XU, J.-J. & DAVIS, S. H. 1983 *Phys. Fluids* **26**, 2880.
XU, J.-J. & DAVIS, S. H. 1984 *Phys. Fluids* **27**, 1102.